Applications of Porous Silicon Thin Films in Solar Cells and Biosensors

Priyanka Singh, Shailesh N. Sharma, and N.M. Ravindra

An overview of the applications of porous silicon (PS) thin films, as antireflection coatings (ARC) in silicon solar cells and transducers in biosensors, is presented. The reflectance spectra of PS films have been compared with other conventional ARCs (such as SiN_x, TiO_2/MgF_2 and ZnS), and optimal PS ARC with minimum reflectance has been obtained. The implementation of PS into an industrially compatible screen-printed (SP) solar cell by both the electrochemical etching (ECE) and chemical etching (CE) methods are reviewed. Porous silicon films, formed via ECE for short anodization times, on textured n^+ emitter of c-Si solar cell having SP front and back contacts, lead to improvements in the performance of solar cells and demonstrate their viability in industrial applications.

INTRODUCTION

Porous silicon (PS) is a sponge-like structure, composed of silicon skeleton permeated by a network of pores. Porous silicon can be obtained by anodization or etching of silicon in aqueous hydrofluoric (HF) solutions and was first discovered in 1956 by Uhlir at the Bell Laboratories.[1] Etching of silicon substrate generates a thin layer of porous silicon on the silicon substrate with pores as large as ~200 nm in diameter (as shown in Figure 1A), providing a large surface area for light trapping (in solar cell applications) and molecular interaction (in sensor applications) inside the porous layer. A scanning electron micrograph of such a PS film which has been formed on crystalline silicon (c-Si) substrate is shown in Figure 1A. The right side images illustrate the magnified top and cross-sectional view of the PS layer and clearly indicate the formed pores of diameter ~200 nm in the PS film.[2] The potential of porous silicon for various technological applications such as optoelectronic devices,[3] displays,[4] photodetectors,[5] and biosensors[6] has been extensively investigated. Such devices can be fabricated by either varying the porosity of the PS film itself or by depositing other films on the PS film such as metals, semiconducting oxides, or polymer films depending on the applications.[7] The large surface-to-volume ratio of porous silicon gives it the ability to react with biochemical species and sense them readily. Recently, PS has attracted more attention due to its sensing properties and has been utilized in chemical, biological[2,6,8–10] and gas[11–17] sensing applications. The advantages of PS sensors are their low cost, ability to operate at room temperature, and compatibility with traditional silicon device fabrication technology. Furthermore, interest in porous silicon in the solar cell industry has grown over the last decade.[18–23]

See the sidebar for a discussion of the formation and morphology of porous silicon.

How would you...

...describe the overall significance of this paper?

An overview of the applications of porous silicon (PS) thin films as antireflection coatings (ARC) in silicon solar cells and transducers in biosensors is presented. The implementation of PS into an industrially compatible screen-printed solar cell by both the electrochemical etching and chemical etching methods are reviewed.

...describe this work to a materials science and engineering professional with no experience in your technical specialty?

The use of porous silicon in solar cells and biosensors is described. In particular, the study focuses on the utility of porous silicon as anti-reflection coatings in solar cells.

...describe this work to a layperson?

In recent years, there has been a growing interest in renewable energy sources. Solar energy represents a non-polluting, naturally available source of energy. Silicon is abundantly available in nature in the form of silica. Silicon solar cells represent the largest component that facilitates the conversion of sunlight to electricity. However, silicon reflects a fraction of the incident light (~33%) which then gets wasted. Anti-reflection coatings help to minimize reflection losses. In the manuscript, we describe the use of porous silicon as an anti-reflection coating.

APPLICATION OF POROUS SILICON AS ARC IN SILICON SOLAR CELLS

As shown in Figure 2A, bare silicon surface reflects more than 30% of the incident sunlight. These reflection losses can be reduced by texturization (it is an important step during solar cell fabrication, which makes silicon surface textured) and by depositing a suitable ARC on the top surface of the solar cell, reflection losses are reduced. This is shown in Figure 2A. The ARC effect relies on destructive interference of waves reflected at the top and bottom of the ARC, as shown in Figure 2B. It can be seen from Figure 2B that PS_1 and PS_2 are two ARCs formed on c-Si solar cell via ECB formation results in a very low reflectance in a certain wavelength range, which for photovoltaic applications must lie between 650 and 700 nm.[24]

For example, in Figure 2A, PS_2 shows ~5% reflectance in the wavelength range of 650 and 700 nm. For an

optimal ARC on a silicon substrate, the required refractive index and thickness is given by:

$$n_{ARC} = \sqrt{n_{Si} n_{air}} \quad (1)$$

$$d_{ARC} = \frac{\lambda_{min}}{4 n_{ARC}} \quad (2)$$

where, n_{Si} is the refractive index of c-Si which depends on wavelength (3.84 at 650 nm, 3.76 at 700 nm), and n_{air} is the refractive index of air. According to Equation 1, the refractive index (n) of an optimized ARC material on silicon should be equal to 1.96 at 650 nm and 1.94 at 700 nm.[28] Hence, from Equations 1 and 2, an ARC thickness (d) of 83 nm (90 nm) is required to produce a zero net reflectance at 650 nm (700 nm).

Table I summarizes the available ARC materials and their refractive indices.[29,30] In order to cover a broad range of the solar spectrum, double layer anti reflection coatings (DLARC) have been investigated by several authors.[31–33] Higher refractive index materials (from 2.2 and 2.6) are preferred as bottom layer films and lower refractive index materials (from 1.3 to 1.6) are generally used as top layer films in DLAR coatings. MgF_2/ZnS, MgF_2/TiO_2, and SiO_2/SiN, have been reported as DLAR coating materials.[34] Canham et al.[24] have established that a PS film used as an ARC should be 60% porous to exhibit an optimal n_{ARC} value. The PS refractive index varies from 1.25 to 3;[24,35] therefore, the additional capability of PS films as single and double layer ARC is evident.

FORMATION AND MORPHOLOGY OF POROUS SILICON

Formation

The most common method for fabricating porous silicon (PS) is the electrochemical etching (ECE) of silicon in HF based electrolyte. The electrolyte contents used for PS formation may vary substantially. However, the electrolyte is generally a mixture of aqueous HF and ethanol (CH_3CH_2OH). Ethanol is used as a surfactant to facilitate extraction of hydrogen bubbles formed during etching.[20,24] Electrochemical anodization is usually performed in an especially designed Teflon cell, using a two-electrode arrangement as shown in Figure 1B. The back of the silicon wafer is held strongly in contact with a metallic copper plate which acts as anode. The PS formation process is performed at a constant current density. The platinum electrode acts as cathode which is positioned in the electrolyte above the silicon surface that is to be etched. The PS film fabricated using this method is generally homogenous in both porosity and thickness.[24]

An alternative method for processing PS is stain or chemical etching (CE) which requires the dipping of silicon substrate in a solution of HF, nitric acid (HNO_3), and water (H_2O). No external bias is used in this process.[24] Nevertheless, the PS formed using this method is inhomogeneous in both porosity and thickness due to the fact that hydrogen gas evolved during formation remains on the surface of the wafer.[25] However, PS formation by stain-etching is particularly attractive because of its simplicity and is useful to produce very thin PS films.[26] Archer[26] has revealed that it is possible to create stain films as thin as 25Å through stain etching with $HF\text{-}HNO_3$ solution.

Morphology

Porous silicon morphology (i.e., pore size, porosity, and pore depth) depends on the type of silicon wafer, its resistivity, method of PS formation (i.e., ECE or CE) and on process conditions such as current density, HF concentration, HF: C_2H_5OH ratio in ECE and $HF:HNO_3$ ratio in CE.[24,27] Figure A shows the morphology of three PS films prepared for HF concentrations of (a) 12.5%, (b) 16.7%, and (c) 25%, in which PS films are prepared by electrochemical etching on p type c-Si wafer. The scanning electron micrograph of the surface of PS film (a), in Figure A, reveals its highly porous nature; film (b) exhibits lower porosity. The top view of the film (c) surface reveals no porous structure even at the largest magnification; on the other hand, many large cracks have been observed. PS films prepared at a current density of 10 mA cm^{-2} and HF concentrations higher than 25% showed surface morphology similar to sample (c).[27]

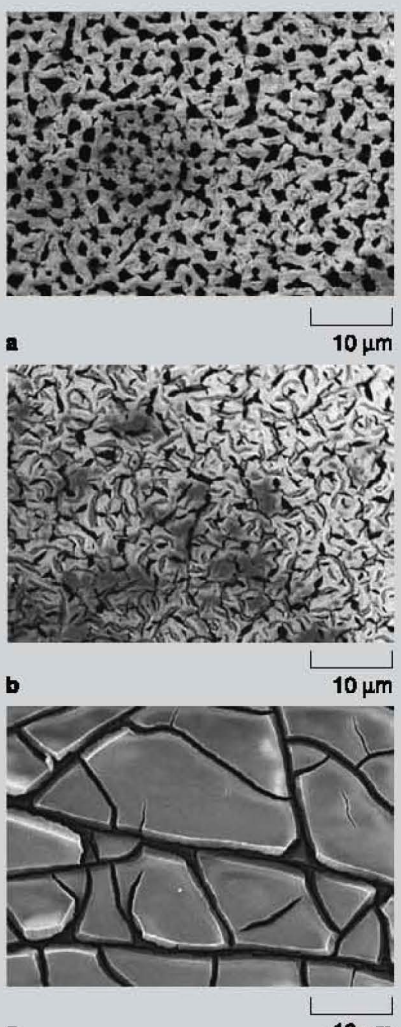

Figure A. Top view scanning electron micrographs of three PS films fabricated in etching solutions with different HF concentrations: (a) 12.5%, (b) 16.7%, and (c) 25%. Anodization current is 10 mA cm^{-2}.[27]

Reflectance of Porous Silicon Films

The comparative analysis of the reflectance spectra of PS films with other conventional ARCs will shed more light on this aspect of PS films. Figure 3 shows the reflectance of PS films along with other ARCs, such as double layer TiO_2/MgF_2, SiN_x and ZnS.[20,35–37] In Figure 3A–C, PS films are formed on n^+ emitter of multicrystalline silicon (mc-Si), SP solar cell. In Figure 3D, PS films are formed on n^+ emitter of SP c-Si solar cell. In Figure 3A, PS films are formed via chemical etching[35] and in Figure 3B–D, PS films are formed via electrochemical anodization using a two-electrode arrangement.[20,36,37] The detailed description of these studies has been presented in the litrature.[20,35–37]

Figure 3A shows the reflectance characteristics of a mc-Si solar cell with (a) PS and (b) double layer (TiO_2/MgF_2) ARC.[20,35] This study has been performed by a group at Fraunhofer-ISE (ISE) on commercial cells from ASE GmbH.[20] The lower reflectance of PS ARC than that of the double layer (TiO_2/MgF_2) ARC, in the wavelength range of ~600–700 nm, clearly exhibits its better anti-reflecting properties for applications in solar cells.[35]

In a recent study by Kwon et al.,[36] the

Table I. Refractive Indices (n) for Various Antireflection Coating Materials Corresponding to Wavelength of 650 to 700 nm[35,20]

Material	Refractive Index (n)
CeO	1.95
CeO_2	2.30–2.40
Al_2O_3	1.60–1.90
Glass	1.50–1.70
MgF_2	1.30–1.40
MgO	1.74
Si_3N_4	1.90
SiO	1.80–1.90
SiO_2	1.46
TiO_2	2.30
Ta_2O_5	2.10–2.30
ZnS	2.33

reflectance of (a) PS ARC is found to be quite comparable to the reflectance of (c) conventional SiN_x ARC on a (b) textured mc-Si in the wavelength range of ~600–700 nm (Figure 3B). It can be seen that PS ARC shows a minimum reflectance of ~3.1% at 570 nm and SiN_x ARC shows a minimum reflectance of ~2.0% at 730 nm. As a result, PS ARC demonstrates optical performance that is superior to vacuum-deposited SiN_x ARC film. In addition, PS is formed uniformly on the entire area of the mc-Si wafer.[36]

The reflectance of a solar cell with an optimized (a) PS ARC and (b) with a SiN ARC is shown in Figure 3C. In this work, PS has been formed on mc-Si solar cells with a very large area (100–164 cm^2). It is clearly seen that similar reflectance is obtained for PS and for the conventional SiN_x ARC.[20] This indicates the advantages of PS as ARC to make solar cells cost effective.

The reflectance spectra of the c-Si solar cells with ARCs (a) PS_1, (b) PS_2, (c) ZnS, and (d) without ARC, in the wavelength range of 360–600 nm are shown in Figure 3D.[37] PS_1 and PS_2 are two porous silicon films deposited on n^+ emitter of c-Si solar cells at different charge densities $Q_1 = 0.06$ C/cm^2 and $Q_2 = 0.9$ C/cm^2, respectively. It can be seen that, in the entire investigated range of wavelengths, the reflectance of the samples with (a) PS_1, (b) PS_2 ARC is less, compared to (c) ZnS ARC and (d) without ARC. It is clear that, in the wavelength range of 550–600 nm, both PS_1 and PS_2 show significantly less reflectance[37] and, hence, PS exhibits good anti-reflecting properties in solar cell applications.

In this work, we have formed PS films via ECE technique in a mixture of HF and C_2H_5OH (1:1 by volume) using Si as the anode and Pt as the counter electrode as shown in Figure 1B. PS has been formed on n^+ textured emitter of c-Si SP solar cell (area~10 cm^2) at varying current density (J-10-40 mA cm^{-2}) and time (t-20 s to 60 s). Figure 2A shows the reflectance spectra of two such PS films; PS_1 and PS_2 along with bare and textured silicon surfaces as a function of wavelength in the range 400–1,100 nm. PS_1 corresponds to current density (J) of 10 $mAcm^{-2}$ and time (t) of 30 s whereas PS_2 corresponds to J = 20 $mAcm^{-2}$ and t = 20 s. It can be seen from Figure 2A that PS_2 ARC shows lower reflectivity values in the most useful part of the solar spectrum (λ_{min}= 650–700 nm) as compared to PS_1. Therefore, it is important to note here that an optimal PS can be obtained by varying current density and time.

These results clearly indicate that PS can be implemented as ARC in industrial solar cells and can possibly replace other conventional single and double layer ARCs.

Application of Porous Silicon in Industrial Solar Cells

Industrial solar cells are generally fabricated on large area (~100 cm^2) Cz c-Si or mc-Si substrates using low-cost processing techniques to obtain a relatively good efficiency at reduced cost. Typical efficiency of commercially produced c-Si solar cells lies in the range of ~13–17%. The efficiency of solar cells depends on processing techniques and influence the production cost at all production stages. Therefore, substantial effort is directed toward efficiency improvement. The industrial solar cell processing steps involve texturization, phosphorous diffusion (to make p-n junction), realization of front and back

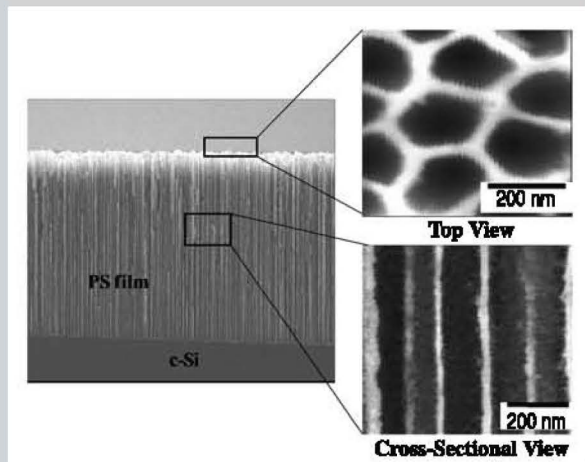

A

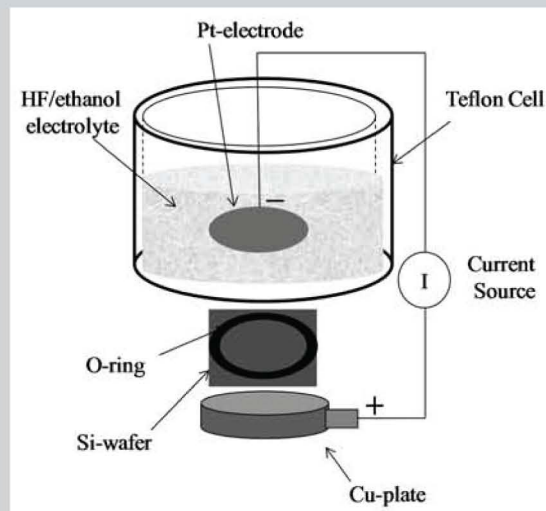

B

Figure 1. (A) SEM image of PS film formed on silicon substrate, the right images, showing the magnified top and cross-sectional view of PS film, clearly shows the pores.[2] (B) The schematic diagram of the cell holder for PS formation. The Si sample is placed on a Cu-plate, which is positively biased, an o-ring (HF-resistant) is placed on top of the sample. The cell material is Teflon. The electrolyte is filled into the reservoir and a Pt-electrode is placed in the electrolyte. The Pt-electrode is negatively biased. A current source controls the current/bias.

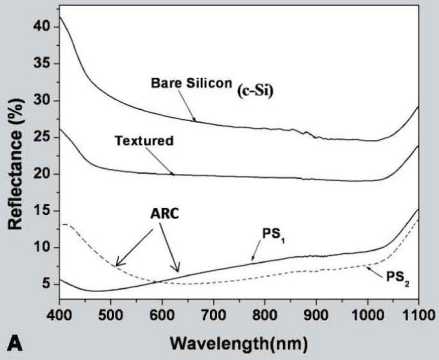

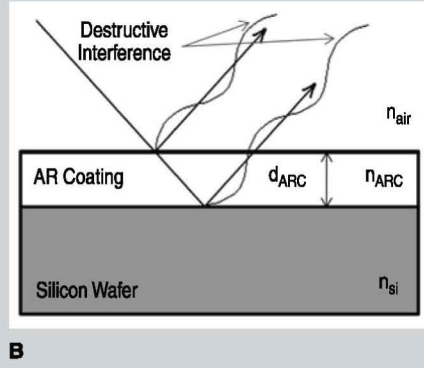

Figure 2. (A) The measured reflectance of the ARCs; PS_1 (J = 10 mA cm^{-2}, t = 30 s) and PS_2 (J = 20 mA cm^{-2}, t = 20 s) formed on c-Si solar cells along with bare and textured silicon surface; (B) principle of anti-reflection coating.

contacts using screen printing techniques followed by deposition of antireflection coating. The schematic representation of one such c-Si solar cell by Sun Power is shown in Figure 4,[38] where the expected solar cell efficiency is ~29%. However, various losses such as reflection, recombination and resistive losses reduce the cell efficiency to 14.7%. It can be seen from Figure 4 that the total losses account for 14.3%, wherein 1.8% of the reflection losses are due to front metallic grid structure and 0.4% reflection losses are after texturization and ARC deposition. The main attraction of porous silicon in the photovoltaic (PV) industry is to use it as a cost effective ARC for large-scale applications. The main advantage of PS as an ARC (as discussed in the preceding section) is well known; it reduces the reflection losses resulting from the silicon surface. Furthermore, PS has a large active area and is capable of light down-shifting in energy or photon energy down-converter (ultraviolet to visible). The use of PS films in solar cells has led to a reduction in the surface recombination velocity, enhancement of the spectral response in the short-wavelength region, and increase in the photogeneration velocity of charge carriers.[18–24] Porous silicon can also serve as a wide bandgap absorber in a multiple-junction cell structure, with c-Si as the substrate.[24] Attempts have been reported to use two PS films with two different bandgaps in a three-bandgap solar cell on a silicon wafer.[39]

Porous silicon ARC formed via ECE or CE on finished solar cells has a serious problem of fill factor degradation due to the increase in series resistance (R_s). Screen printed metalized contacts make direct contact with HF solution during PS formation and therefore degrade the quality of the SP contacts. In order to avoid this degradation problem, the following two approaches can be adopted. In the first approach, ECE can be performed for a short time and this seems to be more convenient for large-scale implementation of PS in finished SP solar cells.[20] In the second approach PS formation can be done on the heavily doped n^+ emitter surface prior to the contact metallization step.[20] However, it is very difficult to obtain a stable ohmic contact on PS layer because of the large surface state density.[40] Therefore, ECE on finished solar cells, for short times seems to be a better option to obtain a homogenous PS ARC. Moreover, in ECE by varying the current density and time, it is possible to obtain PS films with varying refractive indices and thicknesses.[35] Both the methods have been applied to SP silicon solar cells.[20,35,36,41,42] The results of PS ARC implementation using chemical and electrochemical methods in industrial mc-Si solar cell processing are presented in these studies.[20,35,36,41–43] We have formed PS ARC for short anodizaion times via ECE on finished solar cells. Solar cells have been fabricated on c-Si (p-type) wafer using industrial processing steps as described above and have silver fingers on the front side and Ag-Al contact on back side.

A research group at the Università Roma Tre (RM3)[43] and a group from Fraunhofer-ISE (ISE)[35] implemented stain-etched PS ARC on screen printed mc-Si solar cell that is currently used in the PV industry. RM3 used the solar cells from Eurosolare S.p.A.[43] whereas ISE used commercial cells from ASE GmbH.[35] The electrochemical method has been applied by Interuniversity Microelectronics Center, Belgium (IMEC) and Centre National de la Recherche Scientifique–Laboratoire de Physique des Solides de Bellevue (CNRS-LPSB).[20] The efficiency potential of a PS ARC has been investigated by the Interuniversity Microelectronics Center, Belgium on high-quality FZ Si substrates (2×2 cm^2).[20] Centre National de la Recherche Scientifique-Laboratoire de Physique des Solides de Bellevue focuses on the formation of PS ARC for commercial mc-Si solar cells (5×5 cm^2) and the PS film is formed at a constant current density of 50 $mAcm^{-2}$ for 3.5 s. The details of solar cell processing and PS formation are described in the following publications.[20,43] From our recent studies, it is found that the properties of PS formed using screen-printed silver and aluminum as the back contacts are superior as compared to the corresponding films with evaporated back contacts.[44–46] The PS films formed with screen-printed silver and aluminum-back contacts show better crystalline perfection, higher stability, higher Photoluminescence (PL) efficiency and negligible PL decay compared to that formed with evaporated silver and aluminum as the back contact for the same current density and time of anodization. The results conclusively demonstrate the viability of screen-printing contact technology for the possible application of PS films in Si-solar cells.[44–46]

Table II summarizes the measured photovoltaic performance parameters; current density (J_{sc}), open circuit voltage (V_{oc}), fill factor (FF) and efficiency (η) under global AM1.5 illumination for chemical and electrochemical etching on mc-Si solar cells before and after PS formation. In chemical etching, the efficiency of ISE solar cells increases after PS formation; however, the fill factor degraded which may be attributed to the increase in R_s, mainly due to the interaction of HF acid with glass-containing silver paste in SP contacts.[35] In the RM3 cells, the metallization is protected by a polymeric film which explains the smaller degradation of R_s, and hence the achieved higher FF and efficiency.[43] In electrochemical etching, it can be seen from Table II that efficiency of 14.6% and 13.2% has been obtained on the solar cells of IMEC and CNRS-LPSB, respectively. After PS formation, fill

factor does not change in IMEC solar cells, whereas fill factor increases for CNRS-LPSB. The characteristics of the cell (5×5 cm^2 Polix mc-Si) with the PS film (η-13.2%) are similar to commercial cells.[20] Table II also lists the results obtained for optimal PS ARC (PS_2-Figure 2A), implemented on a screen printed c-Si solar cell. It has led to ~20.8% relative improvement in J_{sc}, a significant gain of ~15mV in V_{oc} and a relative increment of about ~.3% in FF. This yields a ~26% increase in efficiency. In a study by Kwon et al.,[36] the optimization of a PS selective emitter in a screen printed mc-Si (2×2 cm^2) solar cell results in a 13.2% efficiency with electroplating.[36]

Thus, PS has immense potential as ARC in commercial solar cell application. Simplicity and low cost of the ECE technique as well as its adaptation to silicon solar cell manufacturing provides a very promising technology in an industrial process.

Characterization of Porous Silicon Films

The surface morphology of PS films has been studied by scanning electron microscope (SEM) and atomic force microscope (AFM). Figure 5A and B shows surface morphology, as seen by SEM and AFM for film PS_2, which has been formed on n^+ emitter of textured c-Si solar cell. As can be seen from Figure 5A, the textured surface shows uniform large pyramids of sizes varying from 1 to 10 μm approximately. The SEM image indicates that the front screen printed silver finger has not been damaged after PS formation. Figure 5B shows three-dimensional (3-D) picture of PS layer, which consists of irregular upright surface features with typical size distribution of ~150–500 nm or even smaller, where the maximum pore size is ~500 nm long and ~50 nm wide whereas the minimum pore size is ~150 nm long and ~30 nm wide. Such types of structures are generally observed in PS films.[24]

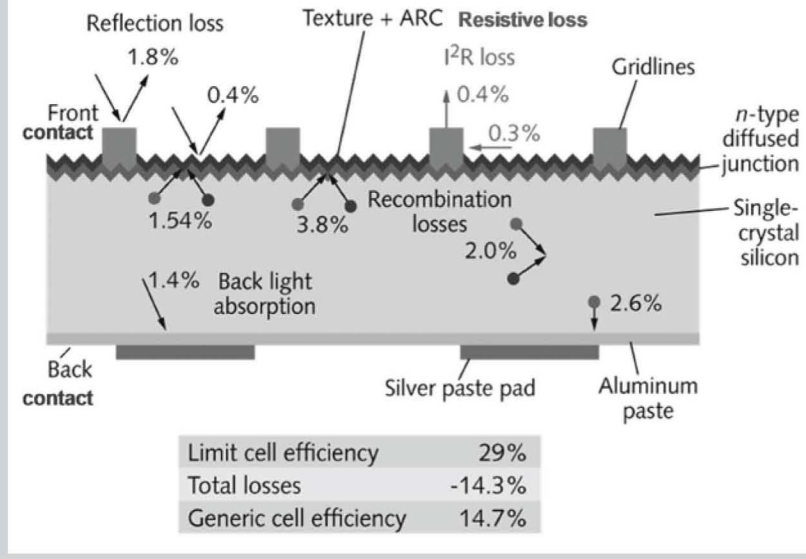

Figure 4. Multiple losses (such as reflection, recombination and resistive) in a single crystal silicon solar cell.[38] (Courtesy of SunPower)

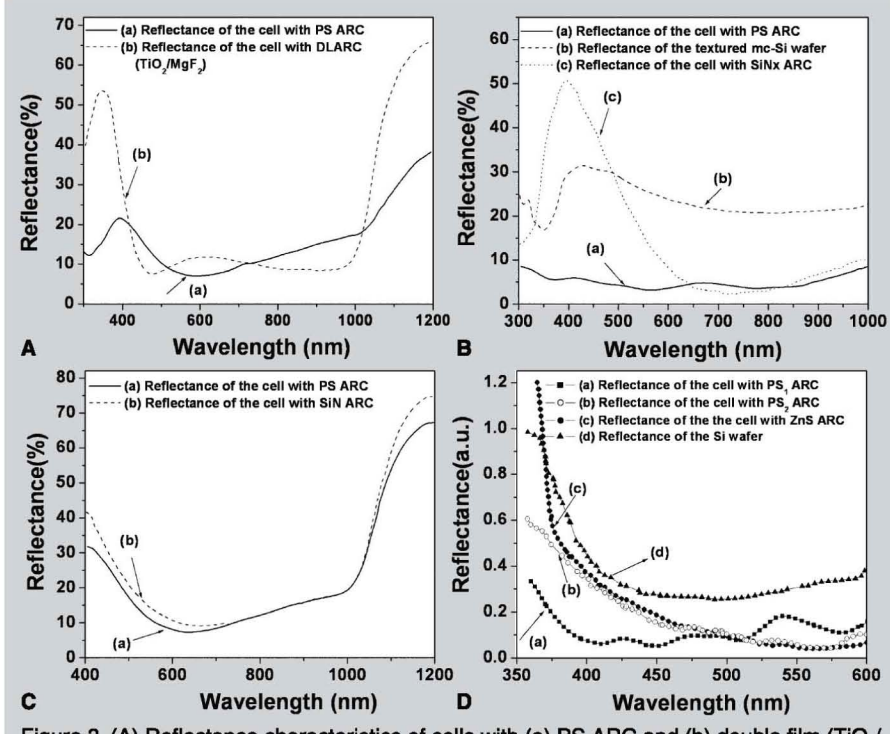

Figure 3. (A) Reflectance characteristics of cells with (a) PS ARC and (b) double film (TiO_2/MgF_2) ARC;[20,35] (B) reflectance characteristics of (a) PS ARC (b) alkaline-textured mc-Si wafer, and (c) single-film SiN_x ARC;[36] (C) reflectance characteristics of mono-Si cells with (a) PS ARC and (b) with conventional SiN ARC;[20] (D) reflectance spectra of samples with ARCs (a) PS_1, (b) PS_2, (c) ZnS and (d) without ARC.[37]

Fourier transform infrared (FTIR) analysis is widely used to characterize the bonding properties in PS films. Here, we present FTIR and photoluminescence (PL) spectra on PS films of various thicknesses, formed on p type c-Si wafer via ECE. In this work, PS films of various thicknesses are formed at optimized current density (J) of 20 mA cm^{-2} with time (t) variation from 1 to 20 minutes, respectively.[45] As current density increases, the thickness of PS film increases.[44] The PS films of various thicknesses, (a)–(e) in Figure 6A and B, are formed at a constant J of 20 mA cm^{-2} and at time t = 1 min, 2 min., 5 min., 20 min., and 30 min., respectively.[45] The thickness of PS films, (a) and (b), are ~150 nm and ~200 nm, respectively, as measured by an ellipsometer; for films (c)–(e), the thickness varies from 5 to 20 μm as estimated from gravimetric measurements.[18] Corresponding FTIR and PL spectra are recorded for these PS films (Figure 6 A and B).

Figure 6A shows the FTIR spectra of PS films of various thicknesses (a)–(e). During PS formation, a large number

of Si-hydride bonds as well as Si-hydroxide bonds are formed and possibly passivate the Si/PS interface.[47] It can be seen in Figure 6A that PS films exhibit mainly Si-H related modes at ~2101 cm^{-1} due to Si-H stretching mode, ~910 cm^{-1} due to Si-H_2 scissors or Si-H_3 symmetric or antisymmetric deformation, doublet ~666 cm^{-1} and 627 cm^{-1} due to Si-H_2 and Si-H wagging while Si-O related modes are marked by very weak signatures at ~1,035 cm^{-1} due to a bulk interstitial Si-O-Si asymmetric stretching model.[18,20,45]

As the thickness of PS films increase (i.e., FTIR spectra from (a)–(e)), a clear increase in both line-width and intensity of these modes can be seen. This indicates the relatively higher hydrogen content in the PS films as thickness increases. However, for very thin PS films, (a), and (b), the FTIR spectra shows only weak signatures of these bands. The distinct presence of Si-H stretching mode at ~2,101 cm^{-1} represents the quality of passivation for PS films (d) and (e). Small peak at ~2,308 cm^{-1} can be related to O back-bonded to Si in Si–H stretching mode.[48] Similar FTIR results on PS films are also discussed in the Reference 20.

Figure 6B shows the corresponding room temperature PL spectra of these PS films (a)–(e). The thin porous silicon film (a) does not exhibit any PL properties which may be attributed to the weak signals of Si-H bands in the FTIR spectra. However, a weak PL can be seen for PS films (b) and (c) which may be attributed to the increase in intensity of Si-H and related bands in the FTIR spectra. The absence of PL properties in PS film (a), and weak PL for films (b) and (c) are apparently due to the silicon skeletons not being narrow enough for quantum confinement. The PL intensity increases as PS film thickness increases (from (a)–(e)) as shown in Figure 6B and a sharp peak at ~688 nm has been obtained for the PS films (d) and (e) corresponding to 10 and 30 minutes of PS formation. The increase in the corresponding normalized PL peak intensity is correlated with the increase in the Si-H and Si-H_2 bonds observed in the FTIR spectra. Therefore, it is worthwhile to note here that SEM, AFM, PL and FTIR studies are important characterization techniques to investigate the structural and passivating properties of PS films.

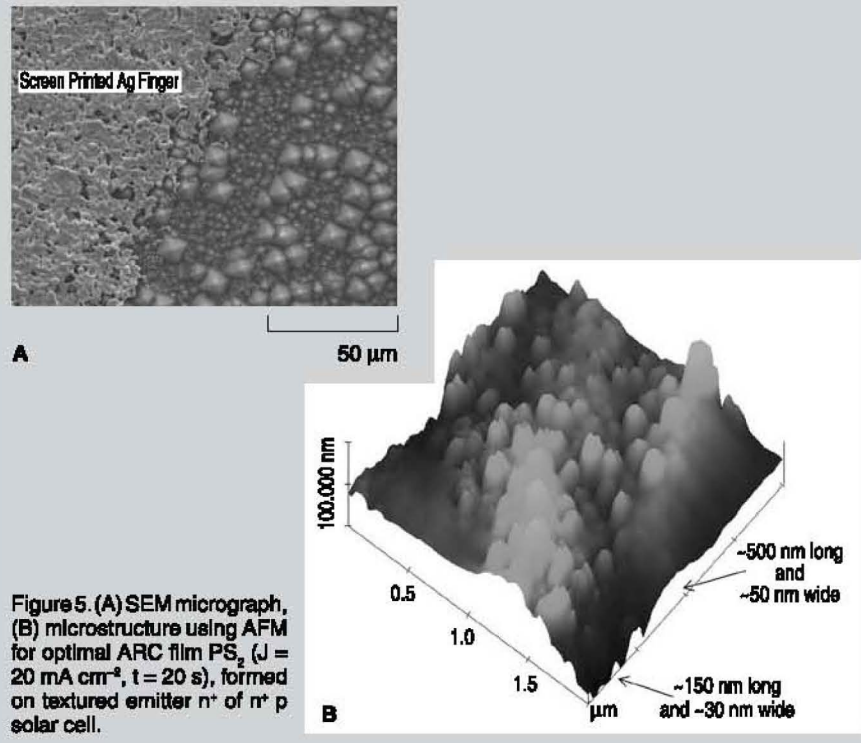

Figure 5. (A) SEM micrograph, (B) microstructure using AFM for optimal ARC film PS_2 ($J = 20$ mA cm^{-2}, $t = 20$ s), formed on textured emitter n^+ of $n^+ p$ solar cell.

APPLICATIONS OF POROUS SILICON IN BIOSENSORS

Biosensors have emerged as highly promising for rapid diagnosis of bacteria in foods. The general function of a biosensor is to convert a biological recognition event into an electrical or optical signal.[49,50] Signal transduction has been accomplished with electrochemical,[51] field-effect transistor,[52] optical absorption, fluorescence and interferometric devices.[53] As discussed previously,[2,6,8–17] a number of theoretical and experimental works, concerning the noteworthy properties of nanostructured porous silicon in chemical and biological sensing, have been reported, showing that, due to its morphological and physical properties, PS is a very versatile sensing platform.[2,6,8–17]

In our recent studies, we observed that PS films formed on textured substrates show higher PL intensity and higher lifetime values as compared to those formed on polished substrates for the same current density.[54] Porous sili-

Table II. Measured Photovoltaic Parameters; Current Density (J_{sc}), Open Circuit Voltage (V_{oc}), Fill Factor (FF), and Efficiency (η) under Global AM1.5 Illumination on Solar Cells using Chemical and Electrochemical PS Formation[20]

PS Process	Cells From	ARC	Area	J_{sc} (cm^2)	V_{oc} ($mAcm^{-2}$)	FF (mV)	η (%)
Chemical	ASE (ISE)	No ARC	100	22.3	575	0.774	9.9
	ASE(ISE) (Eurosolare)	PS ARC	100	28.9	574	0.740	12.3
	RM3	No ARC	164	22.4	588	0.685	9.0
	RM3 (ASE GmbH)	PS ARC	164	27.2	592	0.753	12.1
Electrochemical	IMEC	PS ARC (non-textured)	4	30.4	603	0.78	14.3
	IMEC	PS (textured)	4	31.3	601	0.78	14.6
	CNRS-LPSB	No ARC	25	31.8	595	0.73	13.6
	CNRS-LPSB	PS ARC	25	30.4	583	0.74	13.2
	Present work	No ARC	10	19.7	545	0.67	7.15
	Present work	PS ARC	10	23.8	560	0.68	9.01

con layers and their interfaces have been characterized by recording diffraction curves and measuring lattice mismatch/strain and the radius of curvature due to induced biaxial stress caused by the lattice expansion of PS film due to pores.[55] The higher range of strain values exhibited by PS films on textured specimens corresponding to a wide range of band gaps compared to that formed on polished specimens indicates that stable and higher porosity PS films can be formed on textured substrates at higher current densities. The larger surface area available for PS films formed on textured substrates enables the even distribution of strain, thus, leading to enhanced stability as compared to the corresponding films formed on polished specimens.[55] This factor is responsible for PS films formed on textured substrates to withstand higher strain without any elastic relaxation at high current densities and can be used for gas-sensing measurements.[56] In the case of PS films on polished specimens, the relaxation of the induced strain starts at relatively lower current densities as compared with PS films on textured substrates and thus is not suitable for gas-sensing applications.

The surface of porous silicon needs to be stabilized for biosensing applications and is achieved by means of oxidation, silanization, or hydrosilylation.[57,58] Even without resorting to the above techniques, PS surface can be stabilized using an appropriate post-anodization treatment. At an optimum current density, passivation of defects by a novel nascent-H treatment resulted in the significant enhancement in the PL efficiency.[59] The degraded PL intensity in the treated samples upon prolonged oxidation for several months was higher as compared to that for the as anodized samples. Infrared vibrational studies indicated that the enhancement in PL was due to the H-passivation of defects in the Si-pore interface as also elucidated from capacitance-voltage studies.[59] Furthermore, it has been found that HF-treated PS surfaces are relatively stable against oxidation as compared to untreated PS films.[60] Upon oxidation of the HF treated PS films, the PL intensity initially increases as a result of reduction in crystallite size to exhibit quantum size effects and then decreases owing to loss of luminescing structures due to over-oxidation of the silicon columns. It can be inferred that the surface passivation either by hydrogen or oxygen is one of the requisite conditions for obtaining strong PL efficiency in PS.[61] It seems that more than one emission mechanisms are responsible to explain the luminescence properties of PS.[60]

Furthermore, PS biosensor technology has shown great capability in detecting biological molecules with high selectivity, using specific linker agents and probe molecules.[61] For the biomedical applications of PS, biomolecules have to be first immobilized on its surface through functional groups deposited on it. The common approach is to create a covalent bond between the PS surface and the biomolecules which specifically recognize the target analytes.[61] The reliability of a biosensor strongly depends on the functionalization process as well as its rapidity, simplicity, homogeneity, and repeatability.[62] It is well known that, after anodization, the fresh silicon surface is predominately hydride-terminated which is quite reactive and sensitive to oxidation.[62] Thus, to increase the surface stability of PS, there is a need to functionalize the surface of PS by a suitable precursor. In one of our recent works, nanostructured PS surface was biofunctionalized by thermally depositing thin biocompatible films with a large density of amine groups, using 3-aminopropyltriethoxysilane (APTS) on to its surface.[63] The aim of the study was to demonstrate the covalent bonding between organic molecules (immunoglobulin) and modified inorganic surface (nanostructure PS) which can be used for the detection of protein signals. In this study, PS films prepared at an optimized J~50 mA cm^{-2}, having high PL intensity, stable surface bond configurations, mechanically strong structure and hydrogen-passivated surfaces were used for APTS treatment.[63] The presence of reactive amino groups on the PS surface along with glutaraldehyde as a linker aids in the covalent binding of the antibody (Human IgG) onto the PS surface.[63] Different antigen concentrations can be detected with a good reproducibility with this technique which opens a possibility of using this biofunctionalized material for future biosensors.

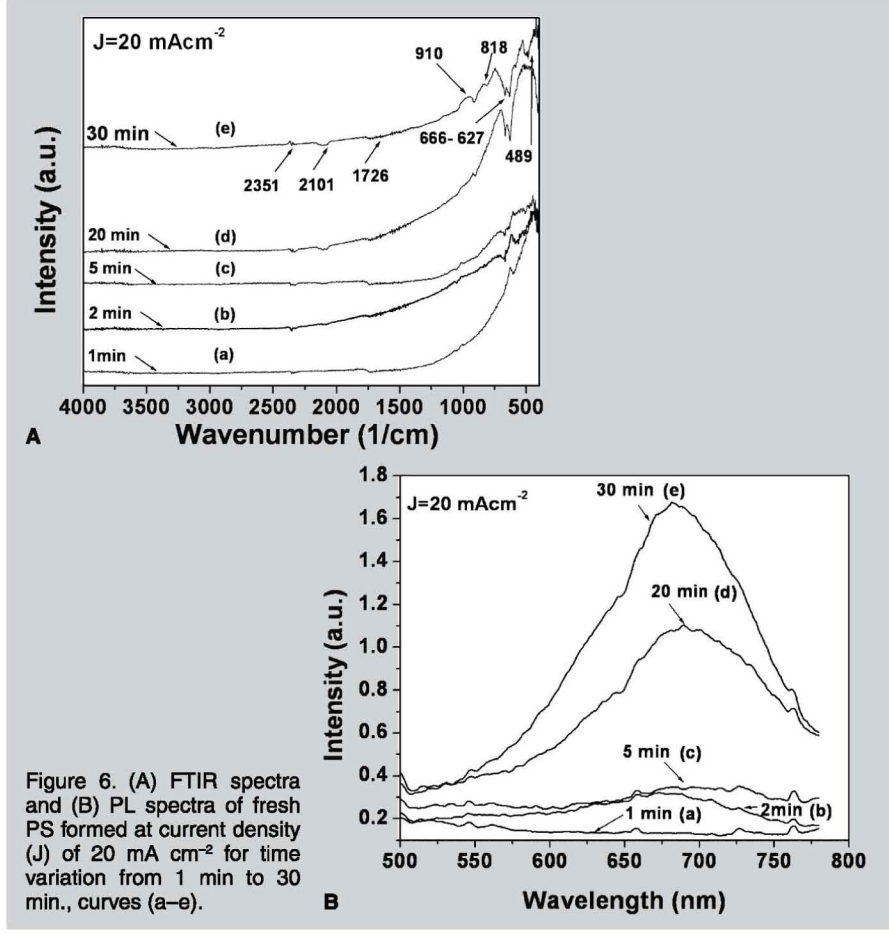

Figure 6. (A) FTIR spectra and (B) PL spectra of fresh PS formed at current density (J) of 20 mA cm^{-2} for time variation from 1 min to 30 min., curves (a–e).

In recent developments, the process of filling the PS pores with metallic, dielectric or semiconducting oxide, enzyme, or molecular receptor films, has resulted in PS sensors that are capable of detecting penicillin, alkali metal ions, humidity, and hydrocarbons.[64] In a paper by Jane et al.,[65] numerous PS biosensors are discussed. One category of biosensor belongs to interference effects in PS single and double layers; the second category discusses the photoluminescence-based transduction; third category is based on PS microcavities and fourth category discusses the electrochemical transduction with porous silicon. The PS biosensors of different categories are compared on the basis of their performance, such as: concentration range, sensitivity for analyte and their detection limit.[65]

Silicon Kinetics has introduced nano PS biosensor and chips to monitor biomolecular interactions,[66] where a nanoporous region has been formed on a c-Si wafer via electrochemical etching. Figure 7A shows the principle of nanoporous biosensor, which is based on the changes in refractive index in the PS layer, when light reflected from the top of the porous region interferes with light reflected from the bottom of the porous region and creates optical interference patterns. The optical path difference signal (OPD signal) is derived from the interferogram as in Figure 7B and rises proportionately with the amount of bound biomolecules. As can be seen in Figure 7B, the first step is to immobilize the first biomolecule of interest i.e., the target on sensor surface (with the desired surface chemistry) and, then, the solution with the second biomolecule of interest i.e., the analyte is introduced; any net binding of the analyte to the target changes the effective index of refraction in the porous region as biomolecules displace buffer solutions with lower indices of refraction.[66]

The simplest example of optical interferometric PS biosensor is shown in Figure 8A[6] which monitors changes in the refractive index that occur in PS single- or double-layer films, wherein PS films are made via electrochemical etching of p type c-Si wafer. In this sensor, binding of molecules induces changes in the refractive index of the porous silicon films.[6] The biosensor has been demonstrated for small organic molecules (biotin and digoxigenin), 16-nucleotide DNA oligomers, and proteins (streptavidin and antibodies) at pico- and femtomolar analyte concentrations. The sensor is also highly effective for detecting single and multi molecular assemblies.[6]

Another example is a porous silicon biosensor chip, fabricated by Mathew et al.,[10] which detects Escherichia coli (E. coli) bacterium and is based on the light emitting properties of porous silicon. In this work, PS films are made via electrochemical etching of p type c-Si wafer and the biosensor adapts single-tube chemiluminescence-based assay for detection of E. coli.[10] The reaction of β-galactosidase enzyme from E. coli with the dioxetane substrate generates light at 530 nm. Figure 8B shows the light emission of a control porous silicon biosensor chip (blank with no E. coli culture) as well as that of porous- and planar-silicon biosensor chips tested with an overnight E. coli pure culture. As shown in Figure 8B, the porous silicon biosensor chip has higher light emissions compared to the planar silicon biosensor chip due to the higher surface area of the porous chip.[10] Sensitivity of the porous silicon biosensor is determined to be 10^1–10^2 colony forming units (CFU) of E. coli.

A potentiometric biosensor for the detection of tryglycerides for metabolomics has been developed by Setzu et al.[67] In this study, PS layers are formed on n^+ type c-Si wafer by electrochemical etching. This biosensor immobilizes lipase enzyme in the PS layer and it induces hydrolysis of a triglyceride, which in turn results in a decrease in the pH and hence shifts the open circuit potential. This approach of immobilization of the enzyme within PS layer considerably increases the working life of the sensor as compared to other lipase-based triglyceride-detection methods.

A label-free optical biosensor for the detection of rabbit IgG (rabbit polyclonal antibody) in whole blood using a PS microcavity has been reported by Bonanno et al.[68] Porous silicon microcavities are formed via ECE into highly doped n-type silicon. Shift in wavelength enables the sensor to detect antibodies in either

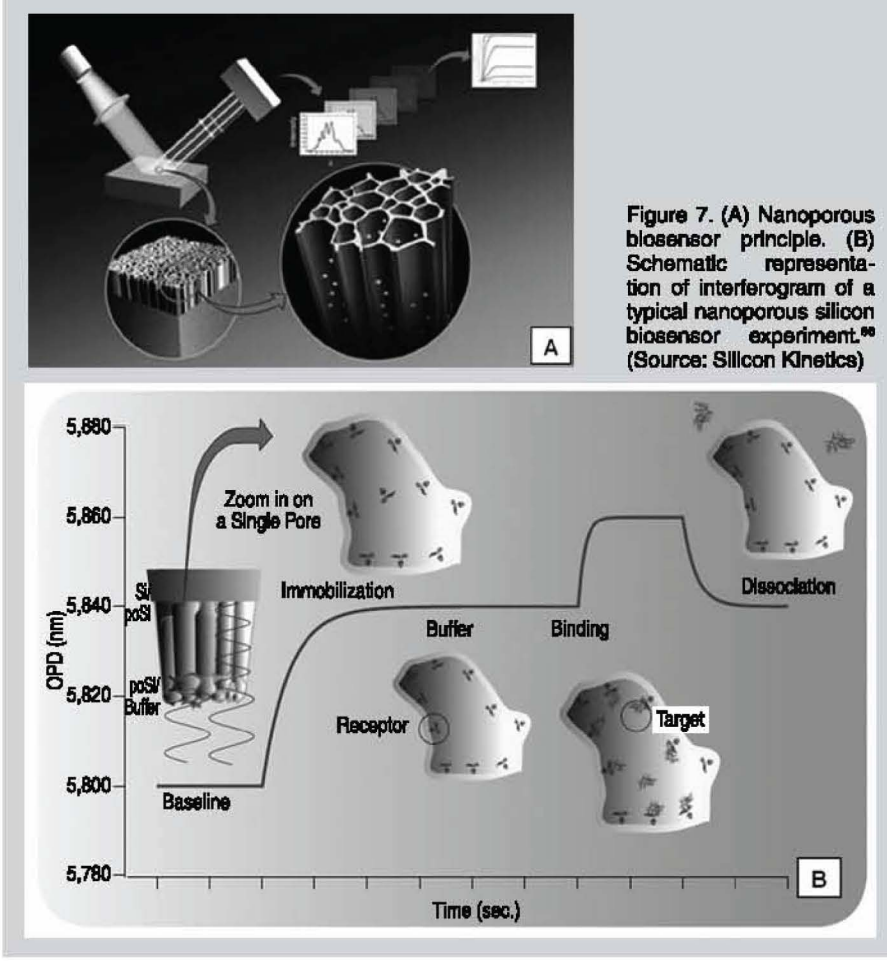

Figure 7. (A) Nanoporous biosensor principle. (B) Schematic representation of interferogram of a typical nanoporous silicon biosensor experiment.[66] (Source: Silicon Kinetics)

undiluted serum or whole blood.[68] Immobilization of antibody on PS surface is done by using biotin-streptavidin. The biosensor has exhibited linear detection range of 2–10 mg/mL.

Another example of PS microcavity sensor has been reported by Ouyang et al.,[69] in which macroporous silicon microcavities were electrochemically synthesized from n-type c-Si wafers. This sensor is operated by analyzing the induced red-shift in the absorbance peak which is caused by the binding of an analyte to an immobilized probe molecule. The device detects an extracellular domain of intimin (intimin-ECB), a protein associated with the pathogenicity of enteropathogenic Escherichia coli. Immobilizition has been carried out by attaching probe molecules: Tir–IBD, the translocated intimin receptor-intimin binding domain, covalently to the PS surface. Intimin-ECB can be detected in a concentration of 4 μM after optimizing the concentration of probe molecules.

Rossi et al.[70] have developed a new method for improving the sensitivity for detection of the bacteriophage virus MS2 using thin films of nanoporous silicon. The PS films are prepared using ECE technique on polished p^+- c-Si wafer. They have shown that a 100 nm thick PS layer with a covalently immobilized antibody has a sensitivity and dynamic range similar to that of the Luminex liquid array-based assay while outperforming protein micro-array methods.[70]

A porous silicon optical biosensor has been developed for monitoring protein-protein binding, specifically protein A with IgG.[71] Thin film of (5 μm) PS has been used for immobilization and transducing matrix and the sensor operates by measurement of the Fabry–Perot fringes in the white light reflection spectrum from the PS layer. Analyte binding causes change in effective optical thickness of functionalized porous silicon Fabry-Perot film and thus transduction is achieved. Sensor demonstrates its stability, reversibility and insensitivity to nonspecific interactions.

Recently, a Fourier transformed reflectometric interference spectroscopy (FTRIFS) PS biosensor has been reported by Shang et al.[72] In this setup, double layers of porous silicon films have been prepared by ECE on p-type c-Si wafers and used as a sensing element for the detection of target molecule by FTRIFS, where trypsin and its inhibitor are used as the model probe-target system. The FTRIFS biosensor has been combined with a UV detector for screening the target molecule from complex component mixtures separated by a LC (liquid chromatography) column, as shown in Figure 9. The outer PS layer, attached with trypsin by amino-silane and glutaraldehyde, can specifically bind with the trypsin inhibitor and acts as a sample channel, while the bottom layer serves as a reference signal channel. The binding event between trypsin and trypsin inhibitor is simultaneously detected by the FTRIFS biosensor in real-time by monitoring the change in optical thickness of the porous silicon layer. Optical signals have a linear relationship with the concentration of trypsin inhibitor in the range of 10–200 ng mL^{-1}.[72]

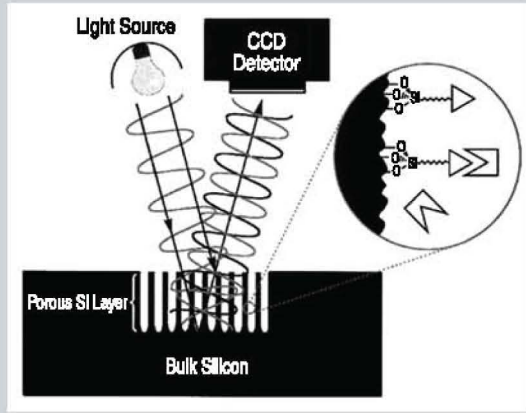

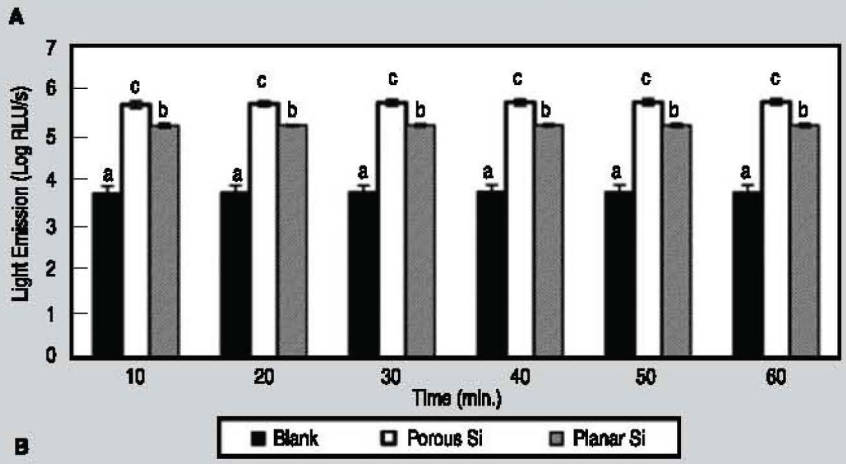

Figure 8. (A) Schematic of PS-based optical interferometric biosensor. Reflection of white light at the top and bottom of the PS film results in an interference pattern. Interactions of molecular species on PS surface induce a change in refractive index of nanocrystalline semiconductor, giving rise to wavelength shifts in fringe pattern that can be easily detected by charge-coupled device (CCD) camera.[9] (B) Comparison of light emission of E. coli pure culture in porous silicon and planar silicon biosensors against porous silicon control.[10]

CONCLUSIONS

Porous silicon has a large potential for applications in photovoltaics. Reflectance of PS film is quite comparable to the reflectance of conventional ARCs (such as SiN_x, double layer TiO_2/MgF_2 and ZnS). The PS film can be easily implemented as ARC into an industrially screen-printed solar cell by both the electrochemical and chemical etching. PS films, formed via ECE for short anodization times are applied on textured n^+ emitter of c-Si having SP front and back contacts. Implementation of optimal PS ARC has led to ~20.8% relative improvement in J_{sc}, a significant gain of ~15 mV in V_{oc} and a relative increment of about ~1.3% in FF. This yields a ~26% increase in efficiency. PS films formed on textured c-Si substrates exhibit higher porosity and PL efficiency, negligible PL decay, better mechanical strength, adherence to the substrate, non-fractured surface morphology and lower stress compared to porous silicon formed on polished c-Si substrates at the same current density and demonstrate the viability of possible application of PS films in Si-solar cells. PS surface morphology on textured emitters in solar cells, as seen by SEM, shows that PS formation does not degrade the unprotected front metallic grid pattern. AFM measurements of PS ARC on textured emitters in solar cells reveal that the maximum pore size is ~500 nm long and ~50 nm wide whereas the minimum

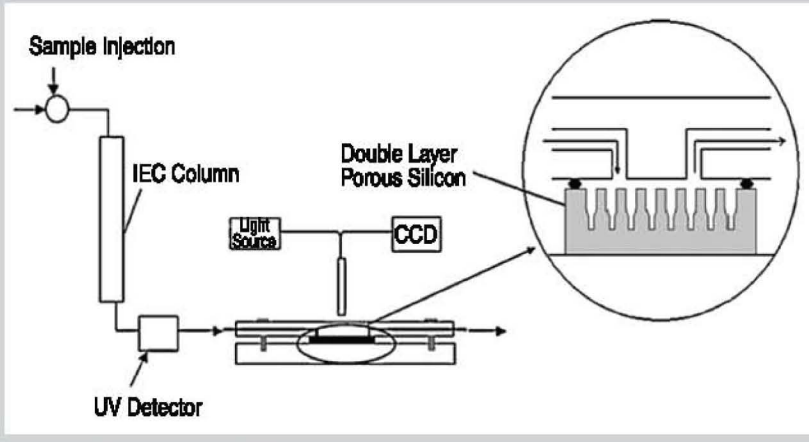

Figure 9. The LC–UV–FTRIFS system, which includes a chromatographic column hyphenated with a UV detector and FTRIFS biosensor in series. A tungsten light source is focused on a porous silicon surface through optical fiber probe, and the interferometric reflectance spectra of porous silicon are collected using a CCD spectrometer coupled to a bifurcated fiber optic cable.[72]

pore size is ~150 nm long and ~30 nm wide. Fourier transform infrared and PL spectra are utilized to characterize the PS films of various thicknesses. Fourier transform infrared results show passivating capabilities of PS films and, therefore, allow fabricating solar cells without an additional passivation coating. The study of the optical properties by PL spectra show that the increase in the PL intensity may be attributed to the presence of Si-H and Si–H_2 bonds with increase in PS film thickness.

Porous silicon biosensors based on optical interferometry and light emitting properties are discussed. For an optimized current density, the functionalization of the PS surface has been achieved by silanization method using APTS as a precursor. The presence of reactive amino groups on the PS surface along with glutaraldehyde as the linker aids in the covalent binding of the antibody (Human IgG) onto the PS surface leading to detection of different antigen concentrations with a good reproducibility.

References

1. A. Uhlir, *Bell Syst. Tech. J.*, 35 (1956), p. 333.
2. H. Ouyang et al., *Adv. Funct. Mater.*, 15 (2005) p. 1851.
3. B. Hamilton, *Semicond. Sci. Technol.*, 10 (1995), p. 1187.
4. V.V. Doan and M.J. Sailor, *Science*, 256 (1992), p. 1791.
5. M.J. Sailor, J.L. Heinrich, and J.M. Lauerhaas, *Semicond. Nanocrystals*, ed. P.V. Kamat and D. Meisel, (New York: Elsevier, 1996), p. 103.
6. V.S.Y. Lin et al. *Science*, 278 (1997), p. 840.
7. V. Parkhutik, *Solid State Electron.*, 43 (1999), p. 1121.
8. L. De Stefano et al., *Sensors*, 7 (2007) p. 214.
9. S.M. Weiss et al., *Opt. Express*, 13 (2005), p. 1090
10. F.P. Mathew and E.C. Alocilja, *Biosensors Bioelectron.*, 20 (2005), p. 1656.
11. F. Besseueille et al., *Biosens. Bioelect.*, 21 (2005), p. 908.
12. C. Pacholski et al., *J. Am. Chem. Soc.*, 127 (2005), p. 11636.
13. K. Watanabe, et al., *Sens. Actuat. B: Chem.*, 33 (1996), p. 194.
14. A. Foucaran et al., *Thin Solid Films*, 297 (1997), p. 317.
15. C. Baratto et al., *Sens. Actuators B: Chem.*, 65 (2000), p. 257.
16. L. Boarino et al., *Mater. Sci. Eng. B*, 69-70 (2000), p. 210.
17. C. Baratto et al., *Sens. Actuators B: Chem.*, 77 (2001), p. 62.
18. A.G. Cullis, L.T. Canham and P.D. Calcott, *J. Appl. Phys.*, 82 (1997), p. 909.
19. S. Bastide et al., *Sol. Eng. Mater. Sol. Cells*, 57 (1999), p. 393.
20. R. R. Bilyalov et al., *Sol. Eng. Mater. Sol. Cells*, 65 (2001), p. 477.
21. A. Krotkus et al., *Sol. Eng. Mater. Sol. Cells*, 45 (1997), p. 267.
22. L. Stalmans et al., *Sol. Eng. Mater. Sol. Cells*, 58 (1999), p. 237.
23. Z. Swiatek et al., *Mater. Sci. Eng. B*, 101 (2003), p. 291.
24. L. Canham, *Properties of Porous Silicon* (London: INSPEC, 1997).
25. K.H. Beckmann, *Surface Science*, 3, (1965) p. 324.
26. R.J. Archer, *J. Phys. Chem. Solids*, 14 (1960), p.14.
27. J. Dian et al., *App. Surf. Sci.*, 238 (1-4) (2004), p. 169.
28. S. Strehlke et al., *Mat. Sci. Eng. B*, 69-70, (2000), p. 81.
29. B.J. Thompson, *Thin Films for Optical Systems* (New York: Marcel Dekker Inc., 1995), p. 295.
30. M.A. Green, *Solar Cells* (Upper-Saddle River, NJ: Prentice-Hall Inc., 1982), p. 164.
31. J. Zhao and M.A. Green, *IEEE Trans. Elect. Dev.*, 38 (1991), p. 1925.
32. Z. Chen et al., *IEEE Trans. Elect. Dev.*, 40 (1993), p. 1161.
33. G. Zhang, J. Zhao, and M.A. Green, *Sol. Eng. Mater. Sol. Cells*, 51 (1998), p. 393.
34. S.E. Lee, S.W. Choi, and J.Yi, *Thin Solid Films*, 376 (2000), p. 208.
35. R.R. Bilyalov et al., *Proc. 26th IEEE Photovol. Spec. Conf.*, (Piscataway, NJ: IEEE, 1997) p. 147.
36. J.H. Kwon, S.H. Lee, and B.K. Ju, *J. Appl. Phys.*, 101 (2007), 104515.
37. Z.N. Adamian et al., *Sol. Eng. Mat. Sol. Cells*, 64 (2000), p. 347.
38. S. Eglash, *Laser Focus World*, 45 (12) (2009), p. 39.
39. L. Kore and G. Bosman, *Sol. Eng. Mater. Sol. Cells*, 57 (1999), p. 31.
40. D. Deresmes et al., *Thin Solid Films*, 255 (1995), p. 258.
41. M. Schnell, R. Lüdemann, and S. Schaefer, Proc. *16th Eur. Comm. Photovol. Sol. Eng. Conf.*, ed. James and James (London: Earthscan Publications Ltd., 2000), p. 1482.
42. R.J. Martin-Palma et al., *Semicond. Sci. Technol.*, 16 (2001), p. 657.
43. L. Schirone et al., *Proc. Sec. World Conf. Photovol. Eng. Conv.*, (1998), p. 276.
44. Priyanka Singh, "Fabrication, Characterization and Other Related Studies for Performance Improvement of Crystalline Silicon Solar Cells" (Ph.D. Thesis, National Physical Laboratory and Jamia Millia Islamia, New Delhi, India, 2008).
45. Priyanka Singh et al., *Sol. Eng. Mat. Sol. Cells*, 9 (2007), p. 1510.
46. P. Singh et al., *Adv. Mater. Res.*, 31 (2008), p. 249.
47. K.H. Jung, S. Shih, and D.L. Kwong, *J. Electrochem. Soc.*, 140 (1993), p. 3046.
48. S.N. Sharma, R.K. Sharma, and S.T. Lakshmikumar, *Physica E*, 28 (2005), p. 264.
49. T.M. Cahn, *Biosensors* (London: Chapman & Hall, 1993).
50. N.M. Ravindra et al., *JOM*, 59 (12), (2007) p. 37.
51. J.J. Hickman et al., *Science*, 252 (1991), p. 688.
52. H.M. McConnell et al., *Ibid.*, 257 (1992), p. 1906.
53. A. Brecht and G. Gauglitz, Biosens, *Bioelectron.*, 10 (1995), p. 923.
54. S.N. Sharma et al., *Mater. Sci. and Eng. B*, 127 (2006), p. 255.
55. G. Bhagavannarayana et al., *Mater. Chem. and Phys.*, 97 (2-3), (2006), p. 442.
56. S.N. Sharma et al., *Physica E-Low-Dimens. Sys. & Nanostru.*, 36 (1), (2007), p. 65.
57. A. Janshoff et al., *J. Am. Chem. Soc.*, 120 (1998), p. 12108.
58. J.M. Buriak et al., *J. Am. Chem. Soc.*, 121 (1999), p. 11491.
59. S. N. Sharma et al., *Appl. Surf. Sci.*, 182 (2001), p. 333.
60. S.N. Sharma, R. Banerjee, and A.K. Barua, *Curr. App. Phys.*, 3 (2003), p. 269.
61. L. Mongo et al., *Anal. Bioanal. Chem.*, 385 (2006), p. 146.
62. L. De Stefano et al. *J. Opt. A: Pure Appl. Opt.*, 8 (2006), p. S540.
63. S. Singh et al., *J. Mater Sci: Mater. Med.*, 20 (2009), p. 181.
64. M.P. Stewart and J.M. Buriak, *Adv. Mater.*, 12 (2000), p. 859.
65. A. Jane et al., *Trends in Biotech.*, 27 (2009), p. 230.
66. Silicon Kinetics, Inc., 10455 Pacific Center Court, San Diego, CA 92121; *www.siliconkinetics.com/*.
67. S. Setzu et al., *Phys. Stat. Solidi A : Appl. Res.*, 204 (2007) p. 1434.
68. L.M. Bonanno and L.A. De Louise, *Biosens. Bioelectron.*, 23 (2007), p. 444.
69. H. Ouyang et al., *Anal. Chem.*, 79 (2007), p. 1502.
70. A.M. Rossi et al., *Biosens. Bioelectron.*, 23 (2007), p. 741.
71. K.P.S. Dancil, D.P. Greiner, and M.J. Sailor, *J. Am. Chem. Soc.*, 121 (1999), p. 7925.
72. Y. Shang et al., *Biosens. Bioelectron.*, 25 (2010), p. 1056.

Priyanka Singh, researcher, and Nuggehalli Ravindra, professor and chair, are with the Physics Department, New Jersey Institute of Technology, 161 Warren Street, Newark, NJ 07102; Shailesh N. Sharma, scientist, is with the National Physical Laboratory, Electronic Materials Division, Semiconductor building, Dr. K.S. Krishnan Marg St., New Delhi 110012, India. Dr. Ravindra can be reached at (973) 596-5742,; fax (973) 596-5794; e-mail nmravindra@gmail.com.